Manipulating the Magnetic Structure of Co Core/CoO Shell Nanoparticles: Implications for Controlling the Exchange Bias

S. E. Inderhees,[1] J. A. Borchers,[2] K. S. Green,[1] M. S. Kim,[1,3] K. Sun,[1] G. L. Strycker,[1] and M. C. Aronson[1,3]
[1]*University of Michigan, Ann Arbor, Michigan 48109-1120, USA*
[2]*National Institute for Standards and Technology, Gaithersburg Maryland 20899-8562, USA*
[3]*Brookhaven National Laboratory, Upton New York 11973, USA*
(Received 26 May 2008; published 9 September 2008)

We present an experimental study of the effects of oxidation on the magnetic and crystal structures of exchange biased ϵ-Co/CoO core-shell nanoparticles. Transmission electron microscopy measurements reveal that oxidation creates a Co-CoO interface which is highly directional and epitaxial in quality. Neutron diffraction measurements find that below a Néel temperature T_N of ~235 K the magnetization of the CoO shell is modulated by two wave vectors, $\mathbf{q_1} = (\frac{1}{2}\ \frac{1}{2}\ \frac{1}{2})\frac{2\pi}{a}$ and $\mathbf{q_2} = (100)\frac{2\pi}{a}$. Oxidation affects the $\mathbf{q_1}$ component of the magnetization very little, but hugely enhances the $\mathbf{q_2}$ component, resulting in the magnetic decompensation of the core-shell interface. We propose that the large exchange bias effect results from the highly ordered interface between the Co core and CoO shell, and from enhanced core-shell coupling by the uncompensated interface moment.

DOI: 10.1103/PhysRevLett.101.117202 PACS numbers: 75.25.+z, 75.50.Tt, 75.75.+a

When a ferromagnet is in close proximity to an antiferromagnet, the direct exchange interaction between the moments in both can create a unidirectional anisotropy which impedes the reversal of the ferromagnetic moment [1,2]. The magnetization loop is subsequently shifted along the field axis by the field H_{EB}, and the coercive field H_C is enhanced. Since this exchange bias effect can be more effective than the magnetocrystalline anisotropy for stabilizing the moments of small ferromagnetic particles, there is much interest in understanding the fundamental physics which controls H_{EB} and in optimizing its magnitude.

Much attention [2–4] has focused on the system of antiferromagnetic (AF) CoO on ferromagnetic (FM) Co, due to its simple bulk crystal and magnetic structures, its availability as both thin film bilayers and core-shell nanoparticles, and its substantial H_{EB}. The most minimal model of the exchange bias effect [1] suggests that H_{EB} could be as large as 5–6 T, although typical values for H_{EB} measured in Co/CoO thin films are less than 0.1 T [2,4–7]. Neutron scattering measurements have established that the magnetic structures and interactions in thin film systems are more complex than those of the simplest models [8]. Domain formation can change the length scales over which the exchange interaction acts [5,9–14]. The exchange coupling depends on the degree of magnetic compensation at the interface [15], determined by the interplay of the magnetic structure, the orientation of the interface plane [6,16], and also by the magnetic roughness of the interface itself [3]. Clearly, it is difficult to optimize all these factors simultaneously.

Nonetheless, H_{EB} in Co core/CoO shell nanoparticles is found to be ~1 T, approaching the simplest theoretical estimate [2,17–20]. The origin of these large values for H_{EB} remains unexplained, and the prospects for future enhancements are uncertain, due to the lack of information about the magnetic structure of core-shell nanoparticles. We report here the first neutron diffraction study of the complex magnetic structure of exchange biased Co-CoO core-shell nanoparticles.

Neutron diffraction measurements were carried out on nanoparticle powders using the BT-2 and BT-9 triple axis spectrometers at the NIST Center for Neutron Research, with a neutron wavelength of 2.35 Å and a pyrolytic graphite analyzer to reduce background. X-ray diffraction experiments were performed on a diffractometer equipped with an image plate detector and graphite monochromatized Mo- $K\alpha$ radiation. The nanoparticles were examined using a High Resolution Transmission Electron Microscope (TEM) at the University of Michigan Electron Microbeam Analysis Laboratory. A Quantum Designs MPMS magnetometer was used to perform magnetization measurements on powders suspended in paraffin. Total Co masses were determined using atomic absorption measurements. We confirmed that the blocking temperature and the exchange and coercive fields are independent of nanoparticle separation, indicating that the exchange bias controls the magnetic dynamics.

Three different batches of ϵ-Co nanoparticles were synthesized via thermal decomposition of $Co_2(CO)_8$ in the presence of oleic acid and trioctylphosphine oxide surfactants [21], and were oxidized in different ways. The most lightly oxidized sample was heated in an air-nitrogen mixture at 60 °C for several hours. A moderate degree of oxidation was achieved by bubbling oxygen through a resuspended powder at 60 °C for several hours, and the most heavily oxidized sample was heated at 100 °C in air for one day. TEM images [Figs. 1(a) and 1(b)] demonstrate the uniform core-shell morphology of the samples, while

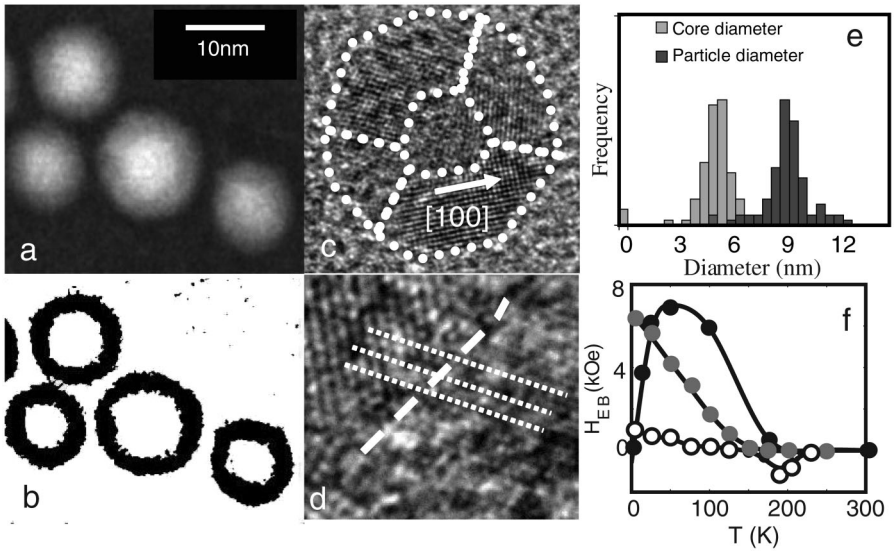

FIG. 1. (a), (b) Z-contrast TEM images of moderately oxidized nanoparticles. (c) TEM image showing crystallinity of Co core and CoO shell. The Co-CoO contact plane is Co (100). (d) TEM image of core-shell interface. (e) Size distributions for core and particle diameters from TEM. (f) The temperature dependence of H_{EB} for light (○, H_{EB} is multiplied by 100), medium (grey circles) and heavily oxidized (●) nanoparticles.

the particle size distribution [Fig. 1(e)] shows that the samples are acceptably monodispersed. We determined the diameter of the ϵ-Co cores from the low temperature saturation moment, assuming the bulk value of 172 emu/gram Co [22]. The particle diameters were determined by direct TEM examination, by small angle x-ray scattering, and by light scattering measurements. The core and shell dimensions are summarized in Table I. We have plotted the temperature dependencies of the exchange fields H_{EB} in Fig. 1(f). While the most lightly oxidized particle has a tiny $H_{EB} \leq 10$ Oe, the moderately and heavily oxidized particles have large values of H_{EB} (6.8 and 6.35 kOe, respectively).

A TEM image of a single Co-CoO nanoparticle which has been moderately oxidized is presented in Fig. 1(c). The ϵ-Co core is truncated by the (100) planes of the Co core. This suggests that oxidation preferentially attacks the exposed (100) planes on the nanoparticle surface, likely obeying the same epitaxial relationship reported for bulk Co surfaces [23], where the (110) axis of rocksalt CoO is parallel to the (100) axis of the underlying Co lattice. A close-up image of the core-shell interface is shown in Fig. 1(d), demonstrating that the registry of rows of Co atoms is uninterrupted through the core-shell interface. The TEM results indicate that the core-shell interface is highly directional and has the low level of disorder characteristic of an epitaxial surface.

Neutron diffraction experiments have been used to study the magnetic and crystal structures of these nanoparticle powders. The temperature evolution of the powder diffraction pattern of the moderately oxidized sample is shown in Fig. 2(a). The two primary peaks present at 325 K can be indexed to the (111) and (200) peaks of the bulk CoO structure, although there is a weak (100) peak at $\mathbf{q_2} = 1.475$ Å^{-1}, normally extinct in the rocksalt structure of bulk CoO. These peaks are also present in the x-ray powder patterns [Fig. 2(c)], and the Scherrer formula indicates that the 0.3 ± 0.05 Å^{-1} widths of the (111) and (200) peaks are consistent with the known dimensions of the CoO shells.

As the temperature is lowered, a new peak emerges at $\mathbf{q_1} = 1.275$ Å^{-1}, corresponding to the bulk CoO AF modulation wave vector $(\frac{1}{2}\ \frac{1}{2}\ \frac{1}{2})2\pi/a$ [24–27]. The intensity of the (100) peak grows with reduced temperature, indicating that it too has a magnetic component. The

TABLE I. Dimensions of the nanoparticle cores and shells.

Degree of Oxidation	Light	Medium	Heavy
Particle Diameter (nm)	7	9	11
Co Core Diameter (nm)	3.9	5.0	3.7
CoO Shell Thickness (nm)	1.6	2.0	3.7

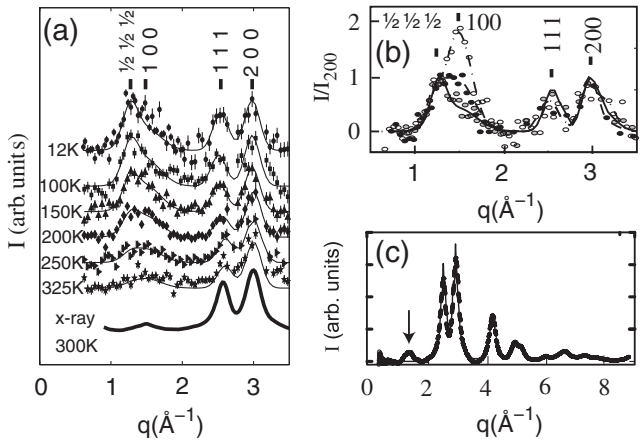

FIG. 2. (a) Neutron diffraction for moderately oxidized particles, as well as the 300 K x-ray diffraction pattern. (b) 12 K neutron powder patterns for lightly (○), medium (gray circles), and heavily (●) oxidized particles, normalized to intensities of the corresponding (200) nuclear peaks. Solid lines are fits to Gaussian line shapes. (c) Comparison of the 300 K x-ray diffraction pattern (gray points) and the refined structure (black line). Arrow indicates (100) peak, omitted from refined structure.

intensities of both the (100) and $(\frac{1}{2}\ \frac{1}{2}\ \frac{1}{2})$ peaks have the temperature dependencies of magnetic order parameters [Figs. 3(a) and 3(b)], indicating $T_N \sim 235$ K for both magnetic modulations in all three samples. This value is much reduced from the 293 K T_N of bulk CoO, presumably by finite size effects such as those observed in CoO thin films [28]. The 0.25 Å^{-1} width of the $(\frac{1}{2}\ \frac{1}{2}\ \frac{1}{2})$ peak is similar to that of the (200) and (111) nuclear peaks, confirming that all three come from the entire CoO shell. The (100) magnetic peak is much broader, and if we neglect strain, the Scherrer formula indicates that it originates in a part of the CoO shell with a thickness of 1.6 ± 0.2 nm in the lightly and heavily oxidized samples, and 1.3 ± 0.1 nm in the moderately oxidized sample. We compare the intensities of the magnetic peaks in all three samples in Fig. 2(b), normalized by the 300 K integrated intensity of the (200) nuclear peak. The intensities of the (100) and $(\frac{1}{2}\ \frac{1}{2}\ \frac{1}{2})$ peaks vary considerably among the three samples, and we will argue below that this is because the magnetic structure of the CoO shell is not spatially uniform and evolves with oxidation.

Both the crystal and magnetic structures of the CoO shell differ in significant ways from their counterparts in bulk CoO. While bulk CoO has the rocksalt structure above T_N, magnetic ordering is accompanied by a large tetragonal distortion and a smaller trigonal distortion, rendering the crystal structure of the ordered phase monoclinic $C2/m$ [27]. We have used this crystal structure to refine the parts of the 300 and 100 K x-ray diffraction patterns obtained on our moderately oxidized nanoparticle sample with $q > 2$ Å^{-1} [Fig. 2(c)]. The parameters determined from the structural refinement at both temperatures are indistinguishable within our experimental resolution. The lattice constants are $a = 0.5040 \pm 0.004$ nm, $b = 0.3003 \pm 0.003$ nm, and $c = 0.2926 \pm 0.0024$ nm, with $\beta = 124.79 \pm 0.03$. This results in a tetragonal distortion $1 - \sqrt{(a^2/2c^2) - \frac{1}{2}} = 0.0082$, which is somewhat smaller than the value of 0.013 found at 5 K in bulk CoO [27]. Further, we deduce an angle of 88.53 degrees between the edges with lattice constants b and c, compared to 89.98 degrees in bulk CoO, implying that the trigonal distortion is substantially larger in the nanoparticle shells than in bulk CoO. We emphasize that the CoO shells display a new crystalline form of CoO, having both the tetragonal and trigonal distortions found only below T_N in bulk CoO. Unlike bulk CoO, there is no change in the nanoparticle crystal structure at T_N.

Since the (100) peak is forbidden in the $C2/m$ symmetry, its appearance in both the 300 K x-ray and neutron diffraction patterns indicates that at least part of the nanoparticle shell has a crystal structure which is qualitatively different from bulk AF CoO. We propose here a very simple model which may be a starting point for a full structural refinement, having the more limited goal of qualitatively explaining key features of our nanoparticle diffraction patterns. The presence of a (100) nuclear peak implies that the body centered Co has been displaced by an amount δ along the [100] direction relative to the rest of the unit cell, which we approximate by the undistorted rocksalt structure. We have calculated the intensities of the primary nuclear peaks as a function of the parameter $x = 2\pi\delta/a$: $I_{100} \propto [1 - \cos(x)]$, $I_{200} \propto [1 + \cos(2x)]$, $I_{111} \propto [1 + \cos(x)]$. The distortion x at 300 K can be determined directly from the experimental ratios of the (100) and (200) neutron diffraction peaks, yielding, respectively, the values of 1.23 ± 0.07, 0.88 ± 0.05, and 0.99 ± 0.14 for the light, medium, and heavily oxidized samples. These results imply that the thinnest oxide layers are highly distorted, most likely from interface strain due to Co/CoO lattice mismatch. As the oxide layer thickens, strains are initially relaxed, as in the moderately oxidized sample. We infer that defects introduced during further oxidation ultimately lead to increased levels of strain and distortion, as in the heavily oxidized sample.

The presence of AF peaks with both (100) and $(\frac{1}{2}\ \frac{1}{2}\ \frac{1}{2})$ indices implies that two separate magnetic modulations must be present in the distorted crystal structure, as in bulk CoO [27,29,30]: $\mathbf{q_1} = \frac{2\pi}{a}(\frac{1}{2}, \frac{1}{2}, \frac{1}{2})$ and $\mathbf{q_2} = \frac{2\pi}{a} \times (1, 0, 0)$. The $\mathbf{q_1}$ modulation leads to a magnetic diffraction peak with intensity $I_{(1/2)(1/2)(1/2)} \propto (p_{1,\perp})^2[1 + \cos(x/2)]$. The $\mathbf{q_2}$ modulation leads to magnetic diffraction peaks at both (100) and (200), with intensities $I_{100,\mathrm{AF}} \propto (p_{2,\perp})^2 \times [1 + \cos(x)]$ and $I_{200,\mathrm{AF}} \propto (p_{2,\perp})^2[1 - \cos(2x)]$. $p_{1,\perp}$ and $p_{2,\perp}$ are proportional to the powder averaged moment perpendicular to the incident momentum for each modulation. For example, $p^2_{1,\perp} = I(\frac{1}{2}, \frac{1}{2}, \frac{1}{2})/I(200)[1 + \cos(2x)]/[1 + \cos(x)]$, where $I(200)$ is the integrated intensity of the 300 K (200) peak. This approach corrects for distortion

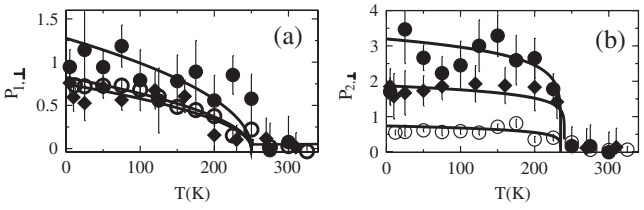

FIG. 3. Temperature dependencies of the moment factors $p_{1,\perp}$ and $p_{2,\perp}$. Light oxidation (●), medium oxidation (○), and heavy oxidation (◆). Solid lines are guides for the eye.

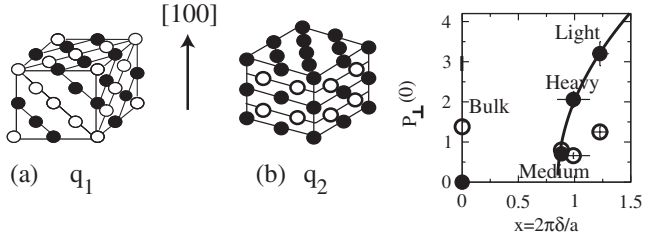

FIG. 4. The $(\frac{1}{2}, \frac{1}{2}, \frac{1}{2})$ (a) and (100) (b) magnetic modulations. Only Co atoms are shown. (c) Zero temperature values of $p_{1,\perp}$ (○) and $p_{2,\perp}$ (●). Bulk CoO has $x = 0$ [24,30].

factors and allows for a direct comparison among samples by accounting for sample mass, neutron flux, and instrumental efficiency. We present the temperature dependencies of $p_{1,\perp}$ and $p_{2,\perp}$ in Figs. 3(a) and 3(b). Both $p_{1,\perp}$ and $p_{2,\perp}$ vanish at T_N, and increase to their maximum value as $T \rightarrow 0$. The zero temperature values of $p_{1,\perp}$ and $p_{2,\perp}$ are reported in Fig. 4(c). The moment factor $p_{1,\perp}$ associated with the $(\frac{1}{2}\ \frac{1}{2}\ \frac{1}{2})$ modulation varies only slightly among the three samples, and is comparable to its value $(1.38)^2 = I_{(1/2)(1/2)(1/2)}/I_{200}$ in bulk CoO [24]. In contrast, the moment factor $p_{2,\perp}$ associated with the (100) modulation is $\sim 10^{-3}$ in bulk CoO [30], but is appreciable in our samples which are above a threshold value of the distortion parameter $x \simeq 0.85$. With further increases in x, $p_{2,\perp}$ continues to grow and rapidly outstrips $p_{1,\perp}$.

As in bulk CoO, the magnetization of our nanoparticles has two different modulation wave vectors: $\mathbf{q_1}$ and $\mathbf{q_2}$ [27,29,30]. Their variations with oxidation have important consequences for the magnetic compensation of the core-shell interface. The $\mathbf{q_1}$ component of the magnetization leads to a component of the AF structure where moments are perpendicular to the (111) planes, with neighboring planes having alternating moment directions [Fig. 4(a)]. By itself, the $\mathbf{q_1}$ structure would lead to a fully compensated (100) plane. Our measurements indicate that the $\mathbf{q_1}$ modulation spans the CoO shell and has an amplitude which is similar to that in bulk CoO. The strains introduced with oxidation seemingly have little impact on the $\mathbf{q_1}$ modulation. In contrast, the $\mathbf{q_2}$ component of the magnetization is almost 1000 times larger than the $\mathbf{q_2}$ component in bulk CoO [30]. By itself, the $\mathbf{q_2}$ modulation would lead to AF order where alternating FM (100) planes are stacked along the [100] axis, leaving the (100) plane completely uncompensated [Fig. 4(b)]. The large width of the (100) magnetic and nuclear peaks indicate that this $\mathbf{q_2}$ modulation derives either from a limited volume of the CoO shell, or from a highly strained region, perhaps the core-shell interface itself. We conclude that the strains introduced by oxidation induce a net rotation of the Co moments relative to the interface. Our primary result is that oxidation renders the Co/CoO interface increasingly uncompensated, steadily increasing the moment induced at the core-shell interface.

Our experiments suggest several reasons why H_{EB} approaches its theoretical estimate in Co/CoO nanoparticles. The Co/CoO interfaces in our nanoparticles are both highly crystalline and highly directional, indicating that interface roughness and defects play only minor roles. In addition, we find that oxidation leads to the decompensation of the (100) CoO surface, and the resulting interface moment enhances the core-shell coupling. We suggest that H_{EB} is small in the lightly oxidized sample because at only 4 unit cells thick, the CoO shell is dominated by the interface. Thus, there is little AF exchange to oppose the coupled reorientation of the moment bearing interface and core. For the moderately and heavily oxidized samples, the CoO shell is delineated into a moment bearing interface as well as a bulklike AF shell. Our results suggest that chemical treatments such as oxidation are promising approaches for manipulating the internal magnetic structure of nanoparticles, a key requirement for optimizing functionality such as the exchange bias effect.

We acknowledge discussions with C. Grey, S. Majetich, J. Rhyne, and J. W. Lynn, and are grateful to C. D. Malliakas and M. G. Kanatzidis for access to their x-ray diffractometer. Work at the University of Michigan and Brookhaven was performed under the auspices of the DOE under Grant DE-FG02-94ER45526.

[1] W. J. Meiklejohn and C. P. Bean, Phys. Rev. **102**, 1413 (1956).
[2] See, for instance, J. Nogues and I. Schuller, J. Magn. Magn. Mater. **192**, 203 (1999).
[3] T. C. Schulthess and W. H. Butler, J. Appl. Phys. **85**, 5510 (1999).
[4] M. Gruyters and D. Riegel, Phys. Rev. B **63**, 052401 (2000).
[5] J. A. Borchers *et al.*, J. Appl. Phys. **83**, 7219 (1998).
[6] N. J. Gokemeijer *et al.*, Phys. Rev. B **63**, 174422 (2001).
[7] B. Beschoten *et al.*, J. Magn. Magn. Mater. **240**, 248 (2002).
[8] M. R. Fitzsimmons *et al.*, J. Magn. Magn. Mater. **271**, 103 (2004).
[9] D. Mauri *et al.*, J. Appl. Phys. **62**, 3047 (1987).
[10] A. P. Malozemoff, J. Appl. Phys. **63**, 3874 (1988).
[11] N. C. Koon, Phys. Rev. Lett. **78**, 4865 (1997).
[12] Y. Ijiri *et al.*, Phys. Rev. Lett. **80**, 608 (1998).
[13] F. Radu *et al.*, Phys. Rev. B **67**, 134409 (2003).
[14] W. T. Lee *et al.*, Phys. Rev. B **65**, 224417 (2002).
[15] K. Takano *et al.*, Phys. Rev. Lett. **79**, 1130 (1997).
[16] R. Jungblut *et al.*, J. Appl. Phys. **75**, 6659 (1994).
[17] S. Gangopadhyay *et al.*, J. Appl. Phys. **73**, 6964 (1993).
[18] D. L. Peng *et al.*, Phys. Rev. B **61**, 3103 (2000).
[19] V. Skumryev *et al.*, Nature (London) **423**, 850 (2003).
[20] J. B. Tracy *et al.*, Phys. Rev. B **72**, 064404 (2005).
[21] V. Puntes *et al.*, Science **291**, 2115 (2001).
[22] *Landolt-Bornstein Numerical Data and Functional Relationships in Science and Technology*, edited by K. H. Hellwege and O. Madelung (Springer, Berlin 1986), Vol. V19A, p. 36.
[23] G. C. Gazzadi *et al.*, Surf. Sci. **402–404**, 632 (1998).
[24] C. G. Shull *et al.*, Phys. Rev. **83**, 333 (1951).
[25] W. L. Roth, Phys. Rev. **110**, 1333 (1958).
[26] B. van Laar *et al.*, Phys. Rev. **138**, A584 (1965).
[27] W. Jauch *et al.*, Phys. Rev. B **64**, 052102 (2001).
[28] T. Ambrose and C. L. Chien, Phys. Rev. Lett. **76**, 1743 (1996).
[29] S. Saito *et al.*, J. Phys. Soc. Jpn. **21**, 850 (1966).
[30] K. Tomiyasu *et al.*, Phys. Rev. B **70**, 184411 (2004).